


Emergent Inductance from Spin Fluctuations in Strongly Correlated Magnets

Taekoo Oh¹ and Naoto Nagaosa^{1*}

RIKEN Center for Emergent Matter Science (CEMS), Wako, Saitama 351-0198, Japan

 (Received 11 August 2023; revised 16 February 2024; accepted 22 February 2024; published 14 March 2024)

Recently, the intriguing phenomenon of emergent inductance has been theoretically proposed and experimentally observed in nanoscale spiral spin systems subjected to oscillating currents. Building upon these recent developments, we put forward the concept of emergent inductance in strongly correlated magnets in the normal state with spin fluctuations. It is argued that the inductance shows a positive peak at temperatures above the ordering temperature. As for the frequency dependence, in systems featuring a single-band structure or a gapped multiband, we observe a Drude-type inductance, while in gapless multiband systems, a non-Drude inductance with a sharp dip near zero frequency. These results offer valuable insights into the behavior of strongly correlated magnets and open up new possibilities for harnessing emergent inductance in practical applications.

DOI: 10.1103/PhysRevLett.132.116501

Introduction.—Noncollinear magnets show a variety of intriguing phenomena such as multiferroics of spin origin [1–3], topological protection of spin textures [4,5], and various kinds of Hall effects [6–12]. The underlying principle of these phenomena is the emergent electromagnetic field [EEMF; magnetic (\mathbf{h}) and electric (\mathbf{e}) fields] [13] associated with the spin Berry connection a_μ ($\mu = 0(t)$, $i = 1, 2, 3$) defined by the spin direction field $\mathbf{n}(r, t)$ as

$$h_i = (\nabla \times \mathbf{a})_i = \frac{\hbar c}{2e} (\varepsilon_{ijk} \mathbf{n} \cdot \partial_j \mathbf{n} \times \partial_k \mathbf{n}), \quad (1)$$

where ε_{ijk} is the totally antisymmetric tensor, and

$$e_i = \frac{1}{c} \frac{\partial a_0}{\partial x_i} - \frac{\partial a_i}{\partial t} = \frac{\hbar c}{2e} (\mathbf{n} \cdot \partial_i \mathbf{n} \times \partial_t \mathbf{n}). \quad (2)$$

According to these formulas, it is theoretically predicted that the coupling of spins of conduction electrons to the spin fluctuation fields induces the emergent inductance in strongly correlated spiral magnets [14]. Later, it is experimentally demonstrated in $\text{Gd}_3\text{Ru}_4\text{Al}_{12}$ [15] and YMn_6Sn_6 [16]. Also, emergent inductance in Rashba spin-orbit-coupled spiral magnets has been theoretically proposed [17].

In respect to the applications, the frequency dependence and the quality factor Q are important issues. At present, the experiments show the rapid decay of inductance as the frequency increases above ~ 10 kHz, and the quality factor Q is less than a few percent. This characteristic frequency is considered to be due to the collective dynamics of the ordered spin system. Typically, the dynamics is characterized by the energy scale αJ , with the Gilbert damping constant α (~ 0.01) and the exchange coupling J of the order of 1 meV. It is noteworthy that the energy scale corresponds to the order of 1 GHz, which is much larger than the

observed one but much smaller than the conduction electrons' that is typically of the order of 1 THz.

Therefore, in the present Letter, we propose a novel mechanism to improve the frequency dependence of the emergent inductance, utilizing the rapid quantum and thermal spin fluctuation in a spin liquid with higher energy than that of ordered moments. To explore this phenomenon, we employ the U(1) slave-fermion theory, where the spin Berry connection \mathbf{a} appears naturally as the phase of the singlet correlation of neighboring spins, which can also be interpreted as the gauge potential. Namely, \mathbf{a} in Eqs. (1) and (2) can be formulated in the slave-fermion gauge theory [18], and its dynamics is given by the current-current correlation function, which determines the physical response. Moreover, in this formalism, the electrons undergo fractionalization into spinons and holons. Importantly, the spinons possess significantly longer lifetimes compared to the holons, leading us to anticipate the emergence of spinonic inductance in the low-frequency regime. Remarkably, the spinon inductance is physically observable according to the Ioffe-Larkin composition rule [19], which is implied by the coupling between spinons and holons through the gauge field \mathbf{a} in the Schwinger boson method [20] or U(1) slave-fermion theory [21].

Our findings, which are illustrated by several systems including a 1D spin chain, 1D spin ladder, 2D square, 2D honeycomb, and 2D kagome lattices, can be summarized as follows. First, we observe that the inductance displays a positive peak at temperatures higher than the “ordering temperature” [see the upper panel of Fig. 1(a)]. Note that the ordering temperature here means the characteristic temperature where the correlation length grows rapidly since there is no long range ordering in 1D and 2D Heisenberg models at finite temperatures. This behavior is attributed to the increased resistivity and inductance as

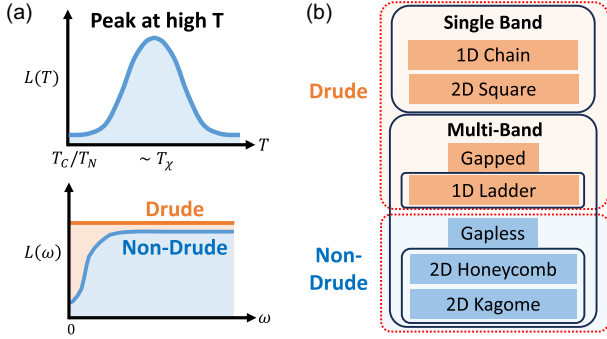


FIG. 1. Our main findings of emergent inductance in strongly correlated magnets at high temperatures. (a) The schematics of inductance in temperatures (upper panel) and in frequencies (lower panel). (b) The classification of inductance: Drude and non-Drude types.

the system becomes less metallic near the spinon phase transition temperature. At much higher temperature, as the system shows the thermally assisted hopping conduction, we anticipate that the inductance lowers down and the peak is found. Second, as for frequency dependence, we distinguish between Drude-type inductance in single-band or gapped multiband systems and non-Drude-type inductance in gapless multiband systems [see Fig. 1(b)]. Drude-type inductance remains independent of frequency, while non-Drude-type inductance exhibits a sharp negative dip near $\omega = 0$, as depicted in the lower panel of Fig. 1(a).

Method.—To investigate the phenomenon of inductance in strongly correlated magnets, we employ the slave-fermion method [22–25]. The behavior of strongly correlated magnets can be effectively captured by the famous t - J model, defined by the Hamiltonian

$$H = -\sum_{\langle ij \rangle} J \left(\mathbf{S}_i \cdot \mathbf{S}_j - \frac{1}{4} n_i n_j \right) - \sum_{\langle ij \rangle} t_{ij} (c_{i\alpha}^\dagger c_{j\alpha} + \text{H.c.}). \quad (3)$$

Within the slave-fermion method, the electron operator can be expressed as $c_{i\alpha}^\dagger = f_{i\alpha}^\dagger b_i + \epsilon_{\alpha\beta} f_{i\beta}^\dagger d_i^\dagger$, subject to the constraint $\sum_\alpha f_{i\alpha}^\dagger f_{i\alpha} + b_i^\dagger b_i + d_i^\dagger d_i = 1$. Here, b_i^\dagger (holon) represents the vacancy, $f_{i\alpha}^\dagger$ (spinon) denotes the single-occupancy with spin α , and d_i^\dagger (doublon) corresponds to the double occupancy. Since the electron is a fermion, either $f_{i\alpha}$ or b_i/d_i must be fermionic, while the other is bosonic. Specifically, when b_i/d_i exhibits fermionic (bosonic) behavior, it is referred to as the slave-fermion (slave-boson) theory.

Because of strong correlation effects, the presence of double occupancy is prohibited. Therefore, the electron operators can be expressed as $c_{i\alpha}^\dagger = f_{i\alpha}^\dagger b_i$, subject to the constraint $\sum_\alpha f_{i\alpha}^\dagger f_{i\alpha} + b_i^\dagger b_i = 1$. Introducing the operators $\hat{\chi}_{ij} = \sum_\alpha f_{i\alpha}^\dagger f_{j\alpha}$ and $\hat{\Delta}_{ij} = \sum_{\alpha\beta} \epsilon_{\alpha\beta} f_{i\alpha}^\dagger f_{j\beta}$, we find that $\mathbf{S}_i \cdot \mathbf{S}_j = \frac{1}{2} [\hat{\chi}_{ij}^\dagger \hat{\chi}_{ij} - 2S(S+1)]$ for ferromagnets, while

$\mathbf{S}_i \cdot \mathbf{S}_j = \frac{1}{2} (2S^2 - \hat{\Delta}_{ij}^\dagger \hat{\Delta}_{ij})$ for antiferromagnets. $\hat{\chi}_{ij}$ represents coherent spinon propagation and $\hat{\Delta}_{ij}$ represents spinon singlet coupling.

By employing slave-fermion mean-field theory (SFMFT) and introducing the order parameters $\chi_{ij} = \langle \hat{\chi}_{ij} \rangle$ in ferromagnets, we arrive at the following Hamiltonian:

$$H = -\tilde{J} \sum_{\langle ij \rangle} (\chi_{ij} \hat{\chi}_{ij}^\dagger + \chi_{ij}^* \hat{\chi}_{ij}) + \sum_{\langle ij \rangle} (t_{ij} \chi_{ij} b_i^\dagger b_j + \text{H.c.}) + \sum_i \lambda_i \left(\sum_\alpha f_{i\alpha}^\dagger f_{i\alpha} + b_i^\dagger b_i - 1 \right). \quad (4)$$

Here $\tilde{J} = J/2$. It should be noted that the last line represents the Lagrange multiplier λ_i associated with the constraint, and the fermionic and bosonic components are treated separately in this formulation.

Using a U(1) gauge theory, the physical conductivity is determined by $\sigma^{-1} = \sigma_f^{-1} + \sigma_b^{-1}$, where $\sigma_{f,b}$ represent the conductivity of spinons and holons, respectively. This is known as the Ioffe-Larkin composition rule [19]. The rule arises from the fact that the spinons flow against holons because of the strong coupling of holons and spinons by the gauge field. We assume that the system is appreciably away from half-filling, so the holon conductivity σ_b follows a Drude-type behavior, $\sigma_b = \sigma_0 / (1 - i\omega\tau_b)$, which is relatively temperature insensitive and much larger than that of spinons. Here, the transport lifetime τ_b is typically $\sim 1 \text{ THz}^{-1} = 1 \text{ ps}$, and the inductance from the holons can be also neglected. Therefore, the remaining part of the Hamiltonian describes the Schwinger-boson theory for the spinons.

Spinons exhibit conductivity at half-filling only in ferromagnetic systems ($J > 0$) since $\chi = \chi_{ij} = 0$ in antiferromagnetic systems ($J < 0$). Thus, we consider the ferromagnetic model on spin chains, honeycomb, and kagome lattices, and determine the order parameters self-consistently at temperatures, as shown in the upper panels of Fig. 2. Subsequently, we compute the current-current correlation function $\Pi(\mathbf{q}, \tau) = -\langle T_\tau J(\mathbf{q}, \tau) J(-\mathbf{q}) \rangle$ and obtain $\text{Re}\sigma(\omega) = -\text{Im}\Pi(\omega)/\omega$ by analytic continuation $i\omega_n \rightarrow \omega + i\eta$. We mostly set $\mathbf{q} = 0$ as the external electric field is constant in space while oscillating in time. The imaginary conductivity is evaluated using the Kramers-Kronig relation, $\text{Im}\sigma(\omega) = -(1/\pi) \int d\omega' [\text{Re}\sigma(\omega') / (\omega' - \omega)]$. The inductivity is then calculated as $\mathcal{L} = -\text{Im}\rho(\omega)/\omega$, where $\rho(\omega) = 1/\sigma(\omega)$. The inductance can be obtained by $L = \mathcal{L}l/A$ where l is the length and A is the area of the system. We set $\tilde{J} = 1$, and present energies and frequencies in units of \tilde{J} . The frequency range is $\omega \in [-3, 3]$ (up to $\sim 1 \text{ GHz}$), and the spinon lifetime parameter is $\eta \approx dk$ where dk is the k -mesh size. We suppose that the system is a cube with 100 nm, so the unit of L is $\sim 0.1 \mu\text{H}$. We will discuss how the units are determined later. Further computational details can be found in the Supplemental Material (SM) [26].

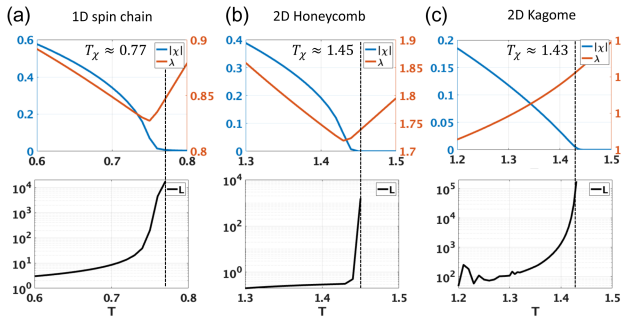


FIG. 2. The order parameters (upper panel) and log-scale inductance (lower panel) in temperatures from the self-consistent SFMFT with $\tilde{J} = 1$ on (a) 1D spin chain, (b) 2D honeycomb lattice, and (c) 2D kagome lattice. T is in units of \tilde{J} , and L is in units of $\sim 0.1 \mu\text{H}$ for the 100 nm cubic sample. The blue lines are the coherent spinon propagation χ , the orange lines are the Lagrange multiplier λ , the black lines are the maximum of inductance L in $\omega \in [-3, 3]$, and the dotted lines denote T_χ .

The inductance peak at high T .—In the upper panels of Fig. 2, the order parameters χ and λ are plotted in temperatures. The phase transition to the finite χ occurs at $T_\chi \approx 0.77$ for the 1D spin chain, $T_\chi \approx 1.45$ for the 2D honeycomb lattice, and $T_\chi \approx 1.43$ for the 2D kagome lattice. The inductance L can only be determined below T_χ by SFMFT, since χ is finite only for this regime. This phase transition is an artifact of the mean-field theory, and describes the crossover from the coherent propagation of the spinons to their thermal hopping conduction. This limitation arises because the model introduces artificial behavior where χ approaches zero at high temperatures and fails to capture the short-range spin correlations which persist at finite values at any finite temperatures [25]. It is also noted that the finite energy gap E_g of the lowest spinon dispersion is similar to or smaller than temperatures below T_χ (see SM).

In the lower panels of Fig. 2, the increased inductance near T_χ within the frequency range $\omega \in [-3, 3]$ is shown. The inductance reaches its highest value $L = 10^3$ – 10^5 near T_χ for every case. Despite the anticipated exaggeration of values from the SFMFT, the incremental (or increasing) tendency of inductance remains true near T_χ . It is important to note that $T_\chi > T_C$ (the Curie-Weiss temperature) considering the presence of short-range spin correlation near T_χ .

Nevertheless, beyond T_χ where SFMFT fails, we anticipate that the inductance decreases with increasing temperatures as the thermally activated hopping motion increases the conductivity. At higher temperatures where lattice vibrations are significant, the spinon transfer could be primarily governed by incoherent thermal excitations. These excitations come from the electron-phonon coupling and the consequent polaron effect which is not included in the present model [27,28]. It is argued that the conductivity

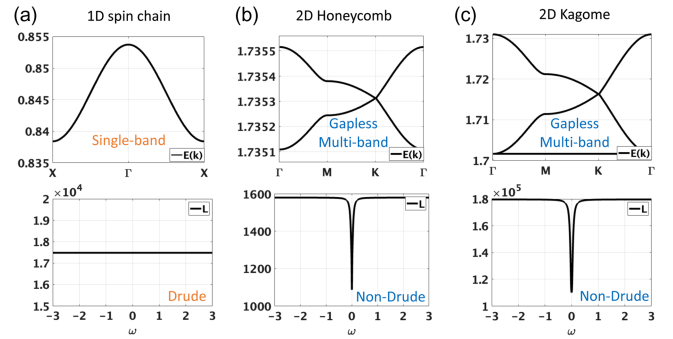


FIG. 3. The energy band (upper panel) and inductance in frequencies (lower panel) near T_χ , for (a) the 1D spin chain, (b) 2D honeycomb lattice, and (c) 2D kagome lattice. $E(k)$ and ω are in units of \tilde{J} , and L has the same unit as above. The 1D spin chain is a single-band system, exhibiting Drude-type inductance. The honeycomb and kagome lattices are gapless multiband systems, exhibiting a sharp negative dip structure near $\omega = 0$.

is at the minimum at the crossover from the coherent propagation to the hopping conduction associated by the phonon. Therefore, the positive peak of the inductance is expected near T_χ .

The inductance in frequencies.—The Drude-type inductance can be briefly reviewed as follows [29]. In a normal metal subjected to an ac electric field $\mathbf{E}(\omega)$, the Drude conductivity is given by $\sigma = \sigma_0 / (1 - i\omega\tau)$, where $\sigma_0 = ne^2\tau/m_e$. Here, n represents the number density, e is the charge of the carriers, τ is the relaxation time, and m_e is the mass of the carriers. Consequently, the resistivity is given by $\rho = (1 - i\omega\tau)/\sigma_0$, and the inductance is given by $L = \tau l / \sigma_0 A = m_e l / ne^2 A$. Importantly, the inductance L remains frequency independent. In the present case, the thermally activated spinons across the gap contribute to the Drude-like transport due to $E_g \lesssim T$.

In the upper panels of Fig. 3, we show the energy band structures near T_χ for the spin chain, honeycomb lattice, and kagome lattice. The 1D spin chain exhibits a single-band structure. In contrast, the 2D honeycomb and kagome lattices are multiband systems with band crossing points, where the interband contribution to the conductivity is also finite. In the honeycomb lattice, the band crossing occurs at the K points. For the kagome lattice, band crossings occur at both the Γ and K points.

In the lower panels of Fig. 3, we present the numerically computed inductance L near T_χ for the spin chain, honeycomb lattice, and kagome lattice. Notably, the inductance exhibits frequency independence only for the spin chain, following a Drude-type behavior. However, for the honeycomb and kagome lattices, the inductance displays a sharp negative dip structure near $\omega = 0$. The characteristics of this sharp dip, including its depth and width, are closely connected to the lifetime parameter η of the spinons. This indicates that the resonance structure is rooted in the transport phenomena of these systems.

The energy gap $E_g \lesssim T$ does not appear in the frequency dependence of the inductance because of the thermally activated bosons. Further details can be found in the SM.

The distinction between the spin chain and other systems arises from the interband transitions at $\mathbf{q} = 0$ in spinon transport. This can be demonstrated through analytic calculations of inductance in two scenarios.

First, consider the 1D spin chain. The current-current correlation function is given by

$$\Pi^1(\mathbf{q}, \omega) = 2(\tilde{J}\chi)^2 \int \frac{dk}{2\pi} \sin^2 k \frac{-\Delta\omega_{k,q}\Delta n}{(\omega + i\eta)^2 - \Delta\omega_{k,q}^2}, \quad (5)$$

where $\Delta\omega_{k,q} = \omega_{k-q/2} - \omega_{k+q/2}$, $\Delta n = n(\omega_{k-q/2}) - n(\omega_{k+q/2})$, and $\omega_k = \lambda - \tilde{J}|\chi| \cos k$ represents the energy. Here, n denotes the Bose-Einstein distribution. Notably, the intraband transition described by $\Delta\omega_{k,q}$ dominates because of a single band in the system. By taking the limits $\eta \rightarrow 0$ and $\mathbf{q} \rightarrow 0$ successively, the total conductivity becomes

$$\sigma^1(\omega) = -2(\tilde{J}\chi)^2 \int \frac{dk}{2\pi} \sin^2 k \left(\pi\delta(\omega) + \frac{i}{\omega} \right) n'(\omega_k). \quad (6)$$

The integration in k yields $\sigma^1(\mathbf{q}, \omega) = A(\pi\delta(\omega) + i/\omega)$ with $A > 0$, rendering the inductance $L = 1/A$ frequency independent.

Second, consider the 2D honeycomb lattice. The current-current correlation function at $\mathbf{q} = 0$ is given by

$$\Pi^2(0, \omega) = 4(\tilde{J}\chi)^2 \int \frac{d^2k}{(2\pi)^2} \frac{\Delta n}{\omega_k} \frac{g(\mathbf{k})^2}{(\omega + i\eta)^2 - (2\omega_k)^2}, \quad (7)$$

where $\mathbf{k} = (k_1, k_2)$, $g(\mathbf{k}) = (\tilde{J}\chi)[1 + \cos k_1 + \cos(k_1 - k_2)]$, $\omega_k^2 = (\tilde{J}\chi)^2[3 + 2\cos k_1 + 2\cos k_2 + 2\cos(k_1 - k_2)]$, and $\Delta n = n(\lambda - \omega_k) - n(\lambda + \omega_k)$. Remarkably, the energy dispersion in the honeycomb lattice is $\lambda \pm \omega_k$, so $2\omega_k = (\lambda + \omega_k) - (\lambda - \omega_k)$ corresponds to interband transitions. Upon performing some algebraic manipulations, we arrive at

$$\sigma^2(\omega) = 2(\tilde{J}\chi)^2 \int_k \frac{g(k)^2 \Delta n}{\omega_k^3} \frac{i(\omega + i\eta)}{(\omega + i\eta)^2 - (2\omega_k)^2}, \quad (8)$$

where $\int_k = \int d^2k/(2\pi)^2$. The integrand exhibits resonance behavior observed in numerical computations. If a band crossing point exists such that $\omega_k = 0$, in the vicinity of $\omega = 0$, the denominator of the integrand approaches zero, leading to a significant increase in conductivity. Consequently, the resistivity decreases near $\omega = 0$, resulting in a sharp negative dip structure in the corresponding inductance.

Three additional aspects are worth noting. First, the result obtained for the 1D spin chain can be generalized to

higher dimensions with a single band. Consequently, we anticipate that higher-dimensional single-band systems would exhibit Drude-type inductance. We briefly address that the 2D square lattice hosts Drude-type inductance in the SM. Second, in a multiband system, the sharp dip structure near $\omega = 0$ may not exist when there is a gap in the energy bands, considering that the denominator in Eq. (8) would not approach zero for such a case. We illustrate it further with a 1D spin ladder model in the SM. Lastly, in the presence of impurities or disorder, even single-band systems or gapped multiband systems demonstrate non-Drude inductance. This arises from the contribution of intraband transitions to the transport phenomenon. We utilize the Mattis-Bardeen scheme [30] in the spin chain, and provide the details in the SM.

Discussion.—In summary, we examine the emergent inductance in strongly correlated magnets with fractionalized spins. At temperatures above the ordering temperature, the dispersion of spinons decreases, leading to a significant increase in inductance. The type of inductance, whether Drude or non-Drude, depends on the system's characteristics such as the number of bands and the presence of band gaps. In non-Drude cases, a sharp dip structure near $\omega = 0$ is observed, and its width is determined by the spinon's relaxation rate, which is typically $\sim J\alpha$ with α being the Gilbert damping constant, and is much smaller than the usual transport relaxation rate τ_b^{-1} .

Here, we discuss the units of physical quantities and the range of the estimated inductance. We assume the unit of exchange interaction J is the order of ~ 1 meV and the unit of lattice constant $a = 1$ Å. Thus, considering that $\hbar = e = 1$, the unit of $k_B T$ is 11.6 K, that of frequency ω is 242 MHz, that of the spinon lifetime η^{-1} is 4.13 ns, that of resistivity ρ is 258 $\mu\Omega$ cm, and that of inductivity \mathcal{L} is 1.07 pH cm. Accordingly, in a cubic system with 100 nm edges, the unit of inductance is approximated ~ 0.1 μ H. Near T_χ , $L \sim 10^2 - 10^4$ μ H, which can be compared to previous experimental findings showing $L \sim 1-10$ μ H [16]. Although the SFMFT exaggerates the computed inductance, we predict that the positive inductance peak at high temperatures is experimentally observable.

Furthermore, it is imperative to consider the impact of electron-phonon interactions, particularly with acoustic phonons, which pervade condensed matters. The electron-phonon interaction plays a significant role in diminishing the emergent inductance. As previously noted, the emergent inductance experiences an increase when spinons exhibit reduced conductivity, resulting in a temperature peak during the transition from coherent to thermal hopping of spinons. We underscore that the transport mechanism at high temperatures is dictated by electron-phonon coupling. Thus, the inclusion of electron-phonon coupling facilitates thermal hopping and thereby reduces the emergent inductance.

Next, we discuss the negative emergent inductance in our system. In a conventional system, the impedance is composed of three components, the inductance \mathbb{L} , the capacitance \mathbb{C} , and the resistance \mathbb{R} . Then, \mathbb{L} should not be negative because of the system's stability. However, the emergent inductance L is the imaginary part of impedance divided by frequency, which is attributed to conventional \mathbb{L} and \mathbb{C} both. Hence, the sharp dip of L near $\omega = 0$ is attributed to \mathbb{C} . When the dip gets sharper, even the negative L emerges. We find the negative L near $\omega = 0$ in our computations on 2D honeycomb lattice at low temperatures (see Fig. S8 in the SM).

We address two necessary conditions for emergent inductance by comparing previous theoretical studies with ours [14,31]. First, the coupling of conduction electron spins to the spin fluctuation fields is required because it gives the spin Berry connection and EEMF. Second, the current-induced spin distortion and relevant energy increase are necessary since the EEMF in Eqs. (1) and (2) is composed of the derivative of spin directions by spacetime.

It is more important to distinguish our Letter from theirs. Both of these studies focus on spiral magnets with weakly correlated electrons, where the EEMF arises from the spin modulation of spiral magnetic order. This stands in stark contrast to our Letter, where we explore spin liquids characterized by ferromagnetic interactions alone. The EEMF in our Letter originates from spin fluctuations within the spin-correlated ground state, without long-range ordering. Here, electrons undergo fractionalization into spinless chargons and neutral spinons due to strong electronic correlations, and the emergent inductance is governed by spinons. In this context, our Letter introduces a novel mechanism for emergent inductance within a spin liquid.

Lastly, we suggest the candidate materials for emergent inductance in addition to $\text{Gd}_3\text{Ru}_4\text{Al}_{12}$ and YMn_6Sn_6 which we already mentioned. The first candidate is the thin film of $\text{La}_{2-x}\text{Ce}_x\text{CuO}_4$. Unlike usual high- T_c cuprates, this system exhibits a ferromagnetic order at higher doping beyond the superconducting dome [32]. Since the system is well described by the t - J model and has a 2D square lattice structure, we anticipate the Drude-type emergent inductance. Other candidates are Cr-based (CrI_3 , CrBr_3 , CrSrTe_3 , CrGeTe_3) and Fe-based $[\text{AFe}_2(\text{PO}_4)_2]$; $\text{A} = \text{Ba}, \text{Cs}, \text{K}, \text{La}$] materials, which are correlated ferromagnets and well described by the spinonic model [33]. Since these materials have a 2D honeycomb lattice structure, we expect the non-Drude-type emergent inductance. We believe that our results provide useful intuitions into the transport in a strongly correlated system complementary to Ref. [31] and reveal the practical prospects for utilizing emergent inductance.

This work was supported by JST, CREST Grant No. JPMJCR1874, Japan.

*nagaosa@riken.jp

- [1] H. Katsura, N. Nagaosa, and A. V. Balatsky, Spin current and magnetoelectric effect in noncollinear magnets, *Phys. Rev. Lett.* **95**, 057205 (2005).
- [2] I. A. Sergienko and E. Dagotto, Role of the Dzyaloshinskii-Moriya interaction in multiferroic perovskites, *Phys. Rev. B* **73**, 094434 (2006).
- [3] A. V. Bezvershenko, A. K. Kolezhuk, and B. A. Ivanov, Stabilization of magnetic skyrmions by Rkky interactions, *Phys. Rev. B* **97**, 054408 (2018).
- [4] T. Schulz, R. Ritz, A. Bauer, M. Halder, M. Wagner, C. Franz, C. Pfleiderer, K. Everschor, M. Garst, and A. Rosch, Emergent electrodynamics of skyrmions in a chiral magnet, *Nat. Phys.* **8**, 301 (2012).
- [5] M. Hirschberger, T. Nakajima, S. Gao, L. Peng, A. Kikkawa, T. Kurumaji, M. Kriener, Y. Yamasaki, H. Sagayama, H. Nakao *et al.*, Skyrmion phase and competing magnetic orders on a breathing kagomé lattice, *Nat. Commun.* **10**, 5831 (2019).
- [6] Y. Taguchi, Y. Oohara, H. Yoshizawa, N. Nagaosa, and Y. Tokura, Spin chirality, berry phase, and anomalous Hall effect in a frustrated ferromagnet, *Science* **291**, 2573 (2001).
- [7] Y. Machida, S. Nakatsuji, Y. Maeno, T. Tayama, T. Sakakibara, and S. Onoda, Unconventional anomalous Hall effect enhanced by a noncoplanar spin texture in the frustrated kondo lattice $\text{Pr}_2\text{Ir}_2\text{O}_7$, *Phys. Rev. Lett.* **98**, 057203 (2007).
- [8] A. Neubauer, C. Pfleiderer, B. Binz, A. Rosch, R. Ritz, P. G. Niklowitz, and P. Böni, Topological Hall effect in the a phase of MnSi , *Phys. Rev. Lett.* **102**, 186602 (2009).
- [9] N. Nagaosa and Y. Tokura, Topological properties and dynamics of magnetic skyrmions, *Nat. Nanotechnol.* **8**, 899 (2013).
- [10] W. J. Kim, T. Oh, J. Song, E. K. Ko, Y. Li, J. Mun, B. Kim, J. Son, Z. Yang, Y. Kohama *et al.*, Strain engineering of the magnetic multipole moments and anomalous Hall effect in pyrochlore iridate thin films, *Sci. Adv.* **6**, eabb1539 (2020).
- [11] Y. Li, T. Oh, J. Song, M. K. Kim, D. Song, S. Kim, S. H. Chang, C. Kim, B.-J. Yang *et al.*, Correlated magnetic Weyl semimetal state in strained $\text{Pr}_2\text{Ir}_2\text{O}_7$, *Adv. Mater.* **33**, 2008528 (2021).
- [12] J. Song, T. Oh, E. K. Ko, J. H. Lee, W. J. Kim, Y. Zhu, B.-J. Yang, Y. Li, and T. W. Noh, Higher harmonics in planar Hall effect induced by cluster magnetic multipoles, *Nat. Commun.* **13**, 6501 (2022).
- [13] S. E. Barnes and S. Maekawa, Generalization of Faraday's law to include nonconservative spin forces, *Phys. Rev. Lett.* **98**, 246601 (2007).
- [14] N. Nagaosa, Emergent inductor by spiral magnets, *Jpn. J. Appl. Phys.* **58**, 120909 (2019).
- [15] T. Yokouchi, F. Kagawa, M. Hirschberger, Y. Otani, N. Nagaosa, and Y. Tokura, Emergent electromagnetic induction in a helical-spin magnet, *Nature (London)* **586**, 232 (2020).
- [16] A. Kitaori, N. Kanazawa, T. Yokouchi, F. Kagawa, N. Nagaosa, and Y. Tokura, Emergent electromagnetic induction beyond room temperature, *Proc. Natl. Acad. Sci. U.S.A.* **118**, e2105422118 (2021).

- [17] J. Ieda and Y. Yamane, Intrinsic and extrinsic tunability of Rashba spin-orbit coupled emergent inductors, *Phys. Rev. B* **103**, L100402 (2021).
- [18] N. Nagaosa, Emergent electromagnetism in condensed matter, *Proc. Jpn. Acad. Ser. B* **95**, 278 (2019).
- [19] L. B. Ioffe and A. I. Larkin, Gapless fermions and gauge fields in dielectrics, *Phys. Rev. B* **39**, 8988 (1989).
- [20] D. P. Arovas and A. Auerbach, Functional integral theories of low-dimensional quantum Heisenberg models, *Phys. Rev. B* **38**, 316 (1988).
- [21] P. A. Lee, N. Nagaosa, and X.-G. Wen, Doping a mott insulator: Physics of high-temperature superconductivity, *Rev. Mod. Phys.* **78**, 17 (2006).
- [22] S. Barnes, New method for the Anderson model, *J. Phys. F* **6**, 1375 (1976).
- [23] P. Coleman, New approach to the mixed-valence problem, *Phys. Rev. B* **29**, 3035 (1984).
- [24] P. A. Lee and N. Nagaosa, Gauge theory of the normal state of high- T_c superconductors, *Phys. Rev. B* **46**, 5621 (1992).
- [25] P. A. Lee, N. Nagaosa, and X.-G. Wen, Doping a mott insulator: Physics of high-temperature superconductivity, *Rev. Mod. Phys.* **78**, 17 (2006).
- [26] See Supplemental Material at <http://link.aps.org/supplemental/10.1103/PhysRevLett.132.116501> for the computational details.
- [27] T. Holstein, Studies of polaron motion: Part I. The molecular-crystal model, *Ann. Phys. (N.Y.)* **8**, 325 (1959).
- [28] J. H. Fetherolf, D. Golež, and T. C. Berkelbach, A unification of the holstein polaron and dynamic disorder pictures of charge transport in organic crystals, *Phys. Rev. X* **10**, 021062 (2020).
- [29] R. Resta, Drude weight and superconducting weight, *J. Phys. Condens. Matter* **30**, 414001 (2018).
- [30] D. C. Mattis and J. Bardeen, Theory of the anomalous skin effect in normal and superconducting metals, *Phys. Rev.* **111**, 412 (1958).
- [31] D. Kurebayashi and N. Nagaosa, Electromagnetic response in spiral magnets and emergent inductance, *Commun. Phys.* **4**, 260 (2021).
- [32] T. Sarkar, D. Wei, J. Zhang, N. Poniatowski, P. Mandal, A. Kapitulnik, and R. L. Greene, Ferromagnetic order beyond the superconducting dome in a cuprate superconductor, *Science* **368**, 532 (2020).
- [33] D. Bhowmick and P. Sengupta, Antichiral edge states in Heisenberg ferromagnet on a honeycomb lattice, *Phys. Rev. B* **101**, 195133 (2020).